Article

Estimation and Assessment of the Root Zone Soil Moisture from Near-Surface Measurements over Huai River Basin

En Liu [1], Yonghua Zhu [1,*], Haishen Lü [1,*], Robert Horton [2], Qiqi Gou [1], Xiaoyi Wang [1], Zhenzhou Ding [1], Haiting Xu [1] and Ying Pan [1]

1 State Key Laboratory of Hydrology-Water Resources and Hydraulic Engineering, College of Hydrology and Water Resources, Hohai University, Nanjing 210098, China
2 Department of Agronomy, Iowa State University, Ames, IA 50011, USA
* Correspondence: zhuyonghua@hhu.edu.cn (Y.Z.); lvhaishen@hhu.edu.cn (H.L.)

Abstract: Root zone soil moisture (RZSM) is a vital variable for agricultural production, water resource management and runoff prediction. Satellites provide large-scale and long-term near-surface soil moisture retrievals, which can be used to estimate RZSM through various methods. In this study, we tested the utility of an exponential filter (ExpF) using in situ soil moisture by optimizing the optimal characteristic time length T_opt for different soil depths. Furthermore, the parameter analysis showed that T_opt correlated negatively with precipitation and had no significant correlation with selected soil properties. Two approaches were taken to obtain T_opt: (1) optimization of the Nash–Sutcliffe efficiency coefficient (NSE); (2) calculation based on annual average precipitation. The precipitation-based T_pre outperformed the station-specific T_opt and stations-averaged T_opt. To apply the ExpF on grid scale, the precipitation-based T_pre considering spatial variability was adopted in the ExpF to obtain RZSM from a new soil moisture dataset RF_SMAP_L3_P (Random Forest Soil Moisture Active Passive_L3_Passive) continuous in time and space over Huai River Basin. Finally, the performance of RF_SMAP_L3_P RZSM (0–100 cm) was evaluated using in situ measurements and compared with mainstream products, for instance, Soil Moisture Active Passive (SMAP) and Soil Moisture and Ocean Salinity Level 4 (SMOS L4) RZSM. The results indicated that RF_SMAP_L3_P RZSM could captured the temporal variation of measured RZSM best with R value of 0.586, followed by SMAP L4, which had the lowest bias value of 0.03, and SMOS L4 significantly underestimated the measured RZSM with bias value of −0.048 in the basin. Higher accuracy of RF_SMAP_L3_P RZSM was found in the flood period compared with the non-flood period, which indicates a better application for ExpF in wetter weather conditions.

Keywords: exponential filter; root zone soil moisture; soil moisture retrievals; soil water balance model

1. Introduction

Soil moisture is a critical state variable in land–atmosphere interactions due to its pivotal role in hydrological cycle, exchange of energy and moisture fluxes, weather and climate systems [1–3]. In particular, root zone soil moisture (RZSM) has important applications in agricultural drought monitoring and prediction, water resource management, and data assimilation for runoff prediction [4–6]. Huai River Basin (HRB) is an important grain production area in China, where floods and droughts occur frequently that seriously threaten agricultural production.

Various techniques (e.g., gravimetric, time/frequency domain reflectometry) provide in situ soil moisture at fixed locations [4,7], so it is hard to map soil moisture at large spatial scale due to high spatial–temporal variability resulting from the interactions and feedbacks between ecohydrological processes. The spatial–temporal variability of soil moisture is crucial for application in water resource management, agricultural production and ecosystem sustainability and is dominated by different factors across different spatial

scales, among which the effect of precipitation distribution on the spatial–temporal soil moisture variability is non-negligible [8,9]. In addition, the relation between the coefficient of variation (CV) of mean spatial soil moisture and mean spatial soil moisture often shows a hysteresis pattern, but the occurrence of hysteresis pattern decreases with increasing spatially soil heterogeneity and even disappears completely for the fully heterogeneous soil [10]. Satellite remote sensing techniques enable us to monitor soil moisture globally, for instance, Soil Moisture Active Passive (SMAP) and Soil Moisture and Ocean Salinity (SMOS). However, they can only capture soil moisture for the top few centimeters (~5 cm) [11–13]. Recently, satellite soil moisture sensing has widely been used. For instance, estimating irrigation magnitude by assimilating satellite soil moisture into the land surface model (LSM) or the soil water balance equation [14]; detecting irrigation signals using satellite soil moisture [15]; retrieving rainfall from satellite soil moisture based on the soil water balance equation [16]; monitoring and predicting extreme events (e.g., agricultural drought and heat waves) [17–20]. Similarly, satellite soil moisture could be used to estimate RZSM due to the strong coupling strength between surface soil moisture (SSM) and RZSM [21–25]. However, quantities of SMAP and SMOS surface soil moisture are missing, spatially affected by radio frequency interference (RFI), especially in Europe and Asia (most areas of China, including the Huai River Basin) [26], which brings great challenges to the application of satellite soil moisture. Therefore, Wang et al. [27] filled the SMAP soil moisture gaps using random forest and created the RF_SMAP_L3_P surface soil moisture, continuous in time and space, which could be used to estimate RZSM over HRB. Both SMOS and SMAP provide continuous spatial and temporal Level 4 (L4) RZSM, but neither have been validated in the HRB and the accuracy is uncertain.

To date, a variety of approaches have been adopted to estimate RZSM from near-surface soil moisture and they are roughly divided into three categories, including (1) statistics-based methods (e.g., linear regression (LR), cumulative distribution function (CDF)) [28,29]; (2) data-driven methods (artificial neural network (ANN)) [30–32]; (3) physics-based methods (e.g., assimilation of remote-sensing data into land surface model, exponential filter (ExpF)) [4,33–36].

Statistics-based methods are the simplest among the three types of methods, which establish the linear relationship between RZSM and SSM or multiple atmospheric forcing variables. However, the accuracy of statistics-based methods is the lowest due to the simple model structure and lack of physical mechanisms. Previous studies show that data-driven methods can predict RZSM with good accuracy, but the disadvantages are obvious: (1) the accuracy of an ANN declines sharply once the data used to predict are outside the training conditions; (2) the trained ANN model has low transferability, limited by local climatic conditions [31,32]. By comparison, physics-based methods are a better choice for the solid physical mechanism and higher accuracy, in which assimilating remote sensing data into the land surface model may be the most accurate [36–38]. However, this method needs a wide range of input data (precipitation, humidity, etc.) and is not suitable for areas where measured data are scarce. In addition, the method has a complex model structure and is computationally expensive. Karandish et al. [39] compare a process-based numerical model (HYDRUS-2D), machine learning (SVM) and multiple regression model (MLR), they reported that process-based numerical models are best at predicting soil moisture, followed by machine learning models and then MLR. Zhang et al. [29] compared three methods (ANN, LR and ExpF) for vertical extrapolation of surface soil moisture and indicated that the ExpF outperforms ANN and LR for capturing the relative variability and correlations between soil moisture at different depths. Tian et al. [2] adopted ANN, CDF and ExpF to estimate subsurface soil moisture from surface soil moisture and reported that ExpF best captures the temporal variation of subsurface soil moisture.

The ExpF was proposed by Wagner et al. [34] on the basis of a two-layer soil water balance equation and widely used to estimate profile soil moisture from near-surface soil moisture with little input and reasonable accuracy at several fixed locations [2,6,11,29,33,35,40]. However, few studies yet exist on estimating RZSM from SSM on a basin scale.

When the ExpF was used to estimate RZSM from satellite-derived soil moisture grid data on a basin scale, it was crucial to obtain the characteristic time length T_opt for each grid unit. Hence, it was necessary to figure out the main controlling factors on T_opt. Albergel et al. [33] pointed that a weak connection between T_opt and climatic conditions may exist. Ford et al. [40] reported that T_opt was sensitive to near-surface soil moisture conditions and tended to be smaller when surface soil moisture conditions were extremely dry or wet. Wang et al. [41] reported that T_opt was negatively correlated with sand fraction and bulk density, and positively correlated with clay fraction and soil organic matter at Automated Weather Data Network (AWDN) stations, but no significant correlation was found at the Soil Climate Analysis Network (SCAN) stations due to the higher spatial variability in precipitation. However, Tian et al. [2] drew the opposite conclusions, namely that T_opt was negatively correlated with clay fraction and soil organic matter, and positively correlated with bulk density. Therefore, the main driver of T_opt may depend on a combination of local specific climatic conditions and soil properties. For the HRB, further research is needed on the main controlling factors of the T_opt and how to derive the T_opt for each grid at basin-scale from the controlling factors.

This study seeks to provide the following information: (1) how to determine the T_opt suitable for the HRB at fixed locations; (2) how to obtain the T_opt with high spatial variability for each grid at basin-scale, considering climatic conditions and soil properties; (3) how to obtain a relatively accurate RZSM dataset for the HRB.

2. Materials and Methods

2.1. Study Area

The Huai River Basin (HRB) is a typical humid and subhumid region in eastern China, bordering the Yellow Sea and covering an area of 27×10^4 km^2. The ranges of longitude and latitude for HRB are 111°55′ to 121°25′ E and 30°55′ to 36°36′ N, respectively (Figure 1). The HRB is located in the transitional zone between northern subtropical (north HRB) and warm temperate climates (south HRB). The average annual precipitation ranges from 600 to 1000 mm with an average of 888 mm, and the annual evaporation ranges from 900 to 1500 mm [42]. There are typical north–south precipitation and evaporation gradients in opposite directions [43–45]. Precipitation is mostly concentrated in June and July. The heterogeneity of precipitation and evaporation leads to dynamic temporal and spatial variations soil moisture; thus, frequent droughts and floods occur in the HRB. The territory is relatively flat, mainly comprising plains surrounded by mountains [42].

2.2. Datasets

2.2.1. In Situ Measurements

The in situ soil moisture measurements were collected at 31 stations from 1 April 2015 to 31 December 2019. At each station, soil moisture is measured daily by time domain reflectometry (TDR) soil moisture probes installed horizontally at depths of 5, 20, 40 and 100 cm. Most of the in situ stations are located on the Huaibei plain where the main land-cover is wheat and maize. Hence, the soil moisture measurements are characterized by similar underlying surface and climate conditions.

Daily precipitation and near-surface air temperature are available on the China Meteorological Data Network (http://data.cma.cn/, accessed on 20 December 2022), and quality control procedures are executed at each station. The grid dataset is obtained by interpolating spatially, using the method of partial thin-plate smoothing splines from more than 2400 national ground meteorological station observations after quality controls and corrections. The average coverage rate of gauging stations located in a grid cell is 38% across the whole of China, but up to 77% in the eastern part of China where the HRB is located. The rainfall data has a mean RMSE of 0.49 mm and R of 0.93 significant at $p < 0.01$ [46]. The air temperature data have a mean bias of ± 0.2 °C and RMSE of 0.2–0.5 °C [47].
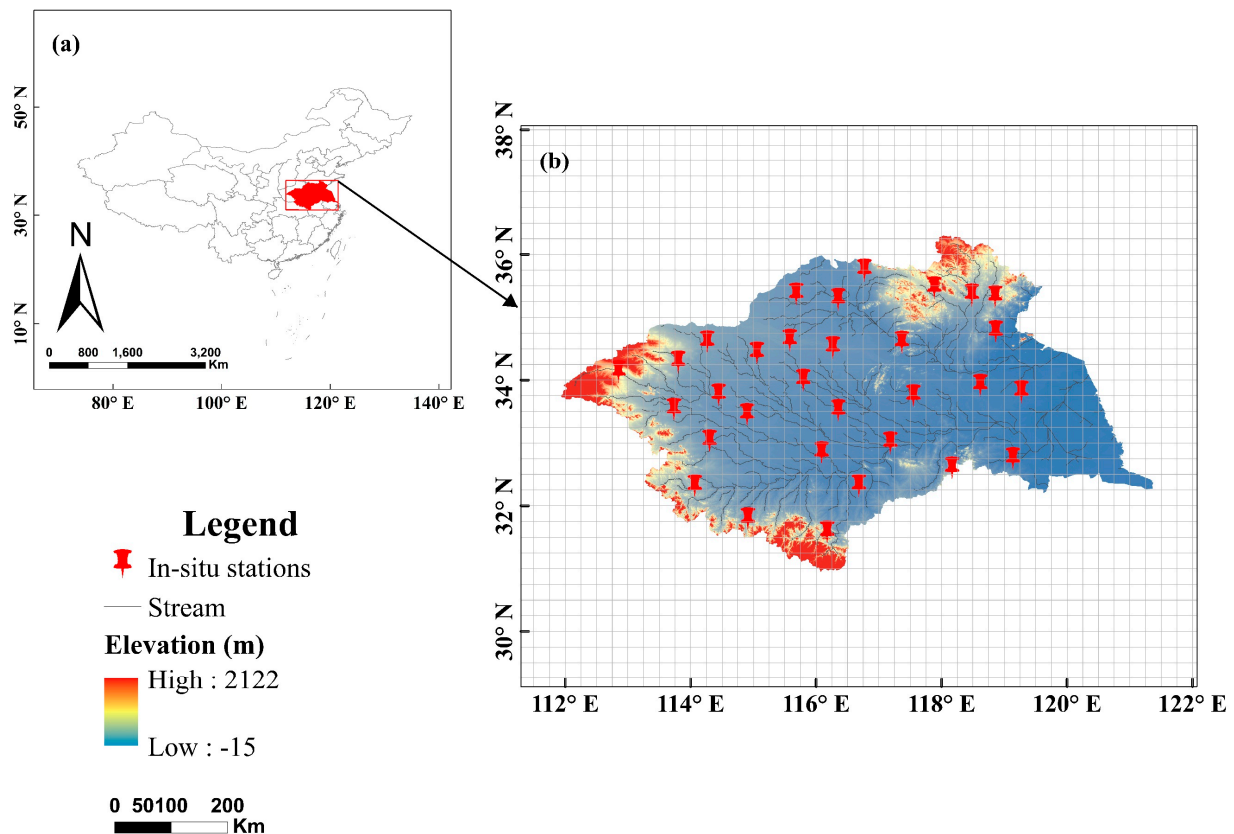
Figure 1. Location of study area (**a**) and distribution of in situ soil moisture stations in the Huai River Basin (**b**), which is divided into a grid of 0.25° × 0.25°. The soil moisture stations probes were buried at depths of 5, 20, 40 and 100 cm.

For soil properties, information of a gridded dataset with a resolution of 30″ × 30″ (about 1 km at the equator) containing the information of eight layers from 0 to 230 cm was compiled using the soil properties from and surface modeling over China [48].

2.2.2. RF_SMAP_L3_P Surface Soil Moisture

The RF_SMAP_L3_P near-surface soil moisture dataset generated by Wang et al. [27] was produced by using NASA-derived data (e.g., soil moisture, precipitation, land surface temperature) to drive a random forest model to estimate missing SMAP values for the Huai River Basin and used as the input for the exponential filter in the study. The RF_SMAP_L3_P near-surface soil moisture dataset has a temporal resolution of 1 day and spatial resolution of 0.25° × 0.25°. The RF_SMAP_L3_P near-surface soil moisture dataset was evaluated with the method of in situ validation (accuracy: ubRMSD ≈ 0.05) and triple collocation analysis (accuracy: ubRMSE ≈ 0.04) by Wang et al. [27], which meets the accuracy requirement of the SMAP mission (0.04 m^3/m^3) for soil moisture retrievals.

2.2.3. SMAP L4 SSM and RZSM Products

The SMAP Level 4 (L4) surface (0–5 cm) and root zone (0–100 cm) soil moisture product is generated by assimilating SMAP L1C_TB brightness temperature data into the NASA Catchment land surface model [49]. The land surface model is driven with surface meteorological forcing data from the Goddard Earth Observing System (GEOS) forward processing system, including corrected GEOS precipitation with the Center for Climate Prediction Unified (CPCU) 0.5° daily precipitation product. The L4 soil moisture product is available from 31 March 2015 to present at a resolution of 9 km and 3 h. The SMAP L4 soil moisture product is distributed by the National Snow and Ice Data Center (NSIDC) (https://nsidc.org/, accessed on 3 January 2023).

2.2.4. SMOS L3 and L4 Products

The SMOS satellite, equipped with a Microwave Imaging Radiometer using an Aperture Synthesis (MIRAS), directly sensed soil moisture in the 0 to 5 cm soil layer. CATDS (Centre Aval de Traitement des Données SMOS) produced and distributed a global, 0.25-degree, daily resolution of the Level 4 root zone soil moisture (L4 RZSM) product from 14 January 2010 to present. The SMOS L4 RZSM (0–100 cm) is obtained from SMOS L3 3-day average SSM (0–5 cm) [13], through a modified formulation of the exponential filter that integrates soil texture. The water bucket model considers the soil profile as three layers (0–5 cm, 5–40 cm and 40–100 cm). The scaled 0–5 cm layer soil moisture was applied to the water bucket model to obtain soil moisture in the of 5–40 cm layer, and a similar procedure is executed for soil moisture in the 40–100 cm layer. The RZSM is depth-weighted average of soil moisture in the three layers. SMOS L3 and L4 products are both available at CATDS (https://www.catds.fr/, accessed on 3 January 2023).

2.3. Methodology

2.3.1. The Recursive Exponential Filter

The exponential filter proposed by Wagner et al. [34] is a two-layer water bucket model, which assumes that the water flux of the two layers is proportional to the difference between SSM and RZSM. Albergel et al. [50] first used a recursive exponential filter equation to estimate RZSM from the remotely sensed surface layer, which is written as:

$$SWI_{m,t_n} = SWI_{m,t_{n-1}} + K_{t_n}\left(ms_{tn} - SWI_{m,t_{n-1}}\right) \tag{1}$$

where SWI_{m,t_n} and $SWI_{m,t_{n-1}}$ are predicted root zone soil wetness index (e.g., 20 cm, 40 cm and 0–100 cm) at times t_n and t_{n-1}, ms_{t_n} is normalized near-surface soil wetness index (5 cm) at t_n, t_n is the time index. ms_{t_n} and SWI_{m,t_n} are both degree of saturation ranging from 0 to 1, which are normalized by daily volumetric soil moisture with maximum and minimum values observed across the entire observation period at each in-situ station, the gain K_{t_n} at time t_n is calculated in a recursive form by:

$$K_{t_n} = \frac{K_{t_{n-1}}}{K_{t_{n-1}} + e^{-\frac{(t_n - t_{n-1})}{T}}} \tag{2}$$

$$T = \frac{L}{C} \tag{3}$$

where T is the characteristic time length in units of day and represents the transfer time from the surface layer to the root zone layer, a comprehensive parameter affected by hydrological processes (precipitation and others) and hydrogeological conditions (soil texture and other properties) [33]. L is the soil layer depth of the root zone, and C is the pseudo diffusion coefficient of soil water. For the initialization of the filter, set $K_1 = 1$ and $SWI_{m,t_1} = ms_{t_1}$, when there is a long time interval between the adjacent observations at time t_n and t_{n-1}, K_n approaches unity, and the new estimate SWI_{m,t_n} takes the value of the new observation ms_{t_n} [51,52]. Finally, SWI values at different depths are rescaled to volumetric water content.

In this study, various T (0–60 days) values were used to optimize the exponential filter, and the optimal T (T_{opt}) value was obtained at each station when the Nash–Sutcliffe efficiency coefficient (NSE) between predicted SWI_m and observed SWI_o peaked. Furthermore, the exponential filter's code, provided by Brocca et al. [53], is available at (Satellite soil moisture validation—hydrology (cnr.it), accessed on 3 January 2023).

2.3.2. Calculation of Profile Soil Moisture (RZSM) Values

The in situ profile soil moisture (0–100 cm) or RZSM is calculated with a depth-weighted method using the soil moisture measured at depths of 5, 20, 40 and 100 cm [54]. The equation is calculated by:

$$\theta_{RZSM} = \frac{2\theta_1 L_1 + (\theta_1 + \theta_2)L_2 + \cdots (\theta_{n-1} + \theta_n)L_n}{2(L_1 + L_2 + L_3 + \cdots L_n)} \quad (4)$$

where θ_{RZSM} is the volumetric soil moisture for the 0–100 cm layer (m^3/m^3), θ_n is the volumetric soil moisture at the nth observation depth (m^3/m^3), and L_n is the soil layer thickness between adjacent observation depths (cm).

2.3.3. Precipitation-Based T_{pre}

We first optimized the station-specific T_{opt} value using in situ measurements at a few fixed locations. However, affected by precipitation, T_{opt} exhibited high spatial variability among the stations. In order to apply the ExpF on each grid unit, we needed to obtain T_{opt} for each grid. T_{opt} was mainly driven by precipitation, so different statistical models, such as linear regression and exponential function, between precipitation and T_{opt} were established to obtain precipitation-based T_{pre} values for each grid from grid precipitation. A summary of the different statistical models is reported in Table S1, and the best fit models are shown below ($R_1 = -0.61$ ***, $R_2 = -0.69$ ***, $R_3 = -0.65$ ***, $R_4 = -0.58$ **, ** denotes that the correlation coefficient R values indicate significant correlation at $p < 0.01$, *** denotes the correlation coefficient R values indicate significant correlate at $p < 0.001$).

$$y_1 = 4013.7e^{-0.006x} \quad (5)$$

$$y_2 = 23290e^{-0.007x} \quad (6)$$

$$y_3 = 27765e^{-0.007x} \quad (7)$$

$$y_4 = 4414.3e^{-0.006x} \quad (8)$$

where y_1, y_2, y_3 and y_4 represent T_{opt} (day) at depths of 20, 40, 100 and 0–100 cm, respectively. x represents annual average precipitation (mm).

3. Results

3.1. The Spatial–Temporal Variability of Soil Moisture

Figure 2a,b displays the evolution of mean spatial soil moisture and coefficient of variation (CV) with time. There is a hysteresis pattern between the CV of spatial soil moisture and mean spatial soil moisture, which could be attributed to differential soil moisture dynamics and lateral flow redistribution and the heterogeneity in soil properties [8,10]. In addition, the root zone soil moisture leads to a slight increase in the occurrence of hysteresis comparing with surface soil moisture in this study. The CV values of spatial soil moisture at depths of 5, 20, 40 and 100 cm across all stations are calculated and are 0.163, 0.150, 0.159 and 0.134, respectively. The root zone soil moisture has a smaller CV than the surface soil moisture, which is significantly affected by strong land–atmosphere interactions. And a smaller CV could lead to an increase in the occurrence of hysteresis. In general, a low precipitation event would mask the hysteresis pattern comparing with a high precipitation event. Figure 2c,d shows the frequency distribution of mean temporal soil moisture and CV of temporal soil moisture. The root zone soil moisture (100 cm) shows similar characteristics to surface soil moisture but has higher range of mean temporal soil moisture (Figure 2c). Figure 2d shows that deeper soil moisture has a smaller range of CV of temporal soil moisture than surface soil moisture and lower frequency distribution. Moreover, the relation between frequency distribution and mean temporal soil moisture shows clear bimodality, but the relation between frequency distribution and CV of temporal

soil moisture shows clear unimodality and being skewed to the smaller CV of the temporal soil moisture.
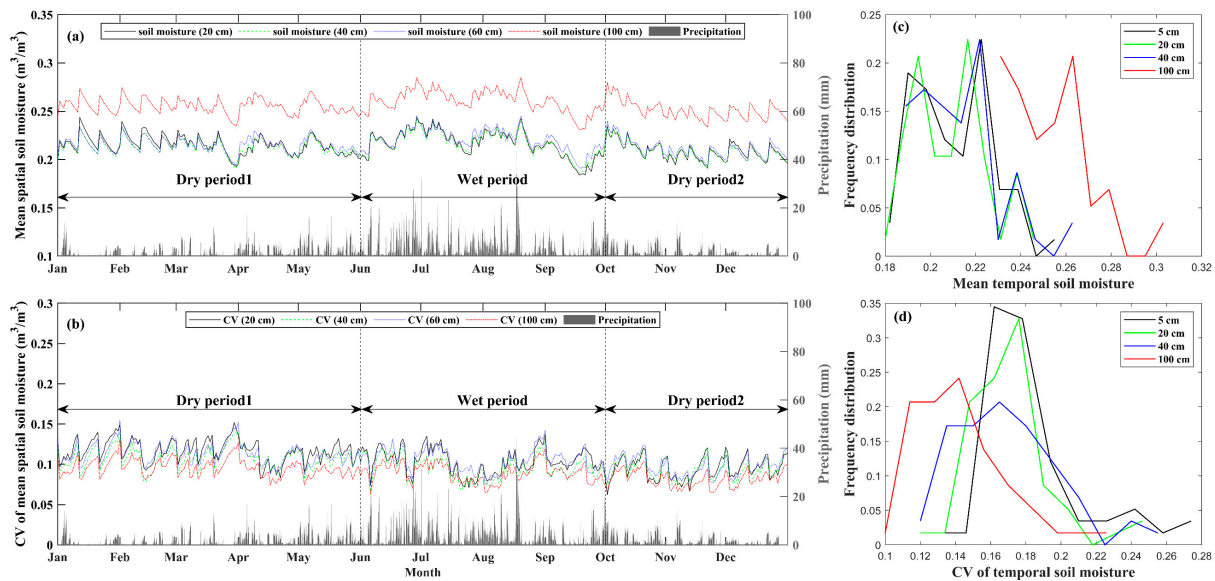
Figure 2. The left panel (**a**,**b**) shows the coefficient of variation (CV) of spatial soil moisture and mean spatial soil moisture at the depths of 5, 20, 40 and 100 cm evolve with time. The right panel (**c**,**d**) shows the frequency distribution of CV of temporal soil moisture and mean temporal soil moisture, respectively.

3.2. Cross Correlation Analysis

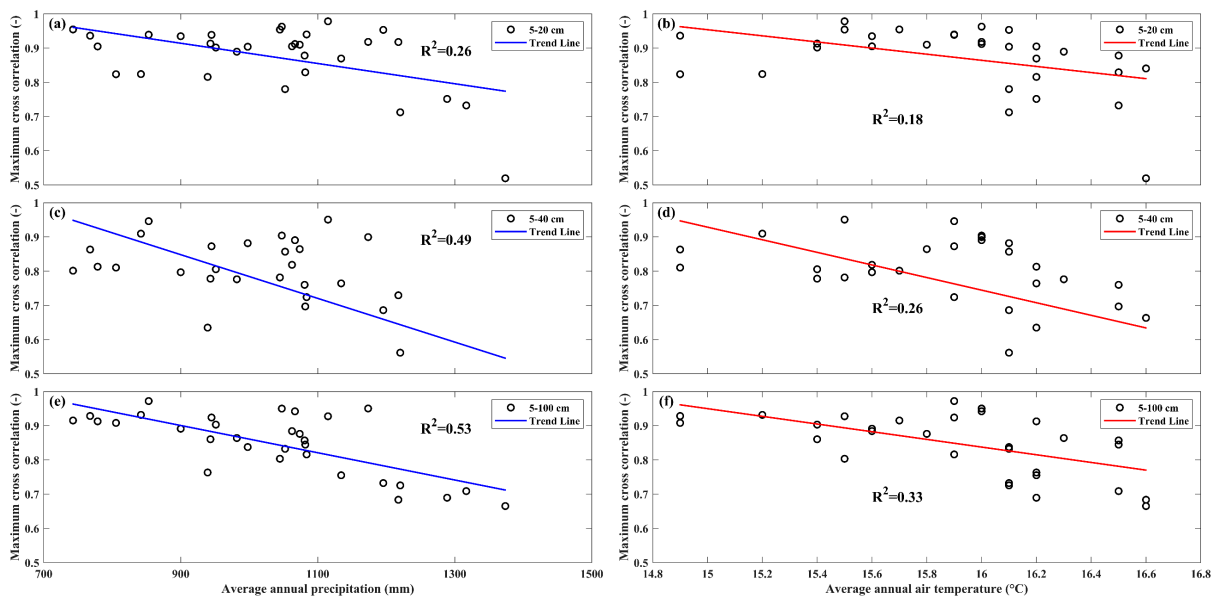#### 3.2.1. Cross-Correlation Coefficient Calculations

Figure 3 displays the cross-correlation coefficients between SSM and RZSM at various depths for selected stations. In general, the coupling strength between SSM and RZSM weakened with time lag (up to 50 days) and soil depth, respectively. The maximum 5–20 cm cross correlation coefficient typically occurred with a 0-day lag and varied from 0.66 to 0.97 with an average value of 0.87 across the study stations. The maximum 5–40 cm cross correlation coefficients were lower than those for 5–20 cm, ranging from 0.52 to 0.90 with an average value of 0.71. The maximum 5–100 cm cross correlation coefficients ranged from 0.32 to 0.54 with an average value of 0.43. The results were consistent with previously reported conclusions [25,40]. In addition, we found an interesting phenomenon. When time lag ranged from 0 to 10 days, the 5–20 cm cross correlation coefficient was higher than those for 5–40 cm and 5–100 cm, respectively. However, for time lags between 10 and 50 days, the 5–100 cm cross correlation coefficients exceeded those for 5–20 cm and 5–40 cm, which could be explained by the fact that response time of the 5–100 cm soil moisture was longer than those for 5–20 cm and 5–40 cm.

3.2.2. Controls on the Coupling Strength

We further analyzed the controlling factors on the coupling strength of soil moisture between SSM and RZSM at various depths. Average annual precipitation, average annual air temperature, relative humidity and evapotranspiration were investigated on how they affected the coupling strength. The relationships between maximum cross correlation coefficients and correlated impact factors are presented in Figure 4. No significant correlation was found between relative humidity, evapotranspiration and maximum cross correlation, so it is not exhibited.
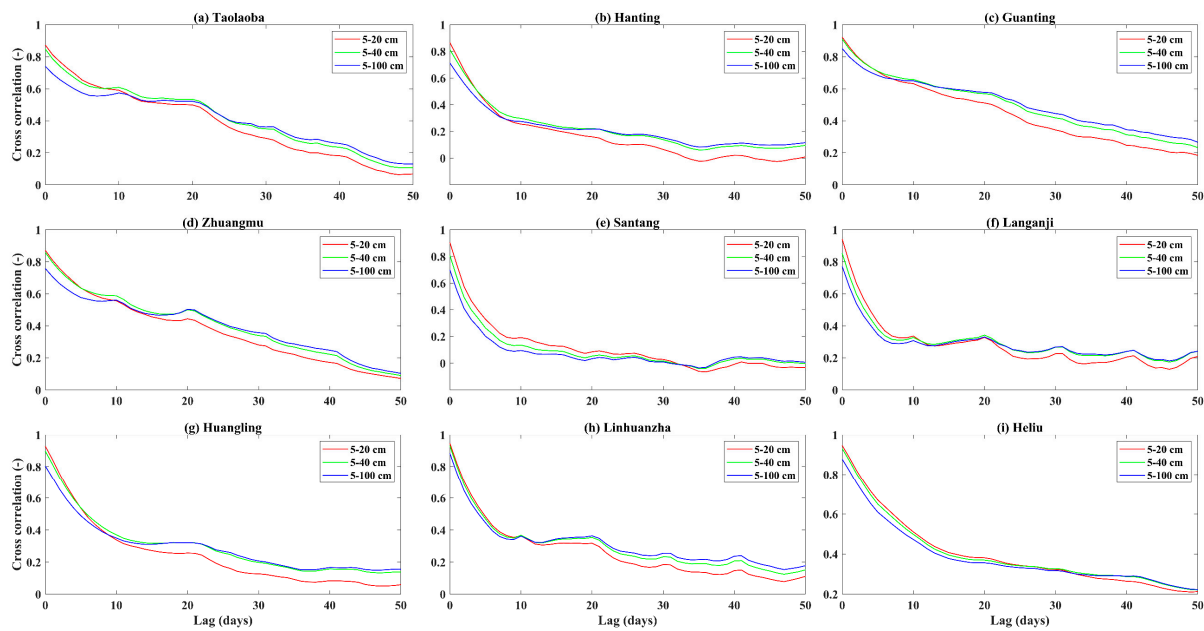
Figure 3. Cross correlation coefficients of soil moisture between near-surface (5 cm) and selected root zone depths (20, 40 and 100 cm) varying with lag time (from 0 to 50 days) at sample stations (**a–i**).

Figure 4. The left panel (**a,c,e**) shows the scatter plots between maximum cross correlation coefficient and average annual precipitation over in situ stations, the right panel (**b,d,f**) is for maximum cross correlation coefficient and average annual air temperature.

The left panel of Figure 4 displays the scatter plots between maximum cross correlation coefficient and average annual precipitation calculated with the daily observations over all in situ stations. There was a significant negative correlation between precipitation and soil moisture coupling strength of 5–20 cm ($R^2 = 0.26$), 5–40 cm ($R^2 = 0.49$) and 5–100 cm ($R^2 = 0.53$), respectively. Moreover, it seemed that precipitation had a stronger influence on the coupling strength between SSM and deeper RZSM. The negative correlation between cross correlation coefficient and average annual precipitation indicated that the coupling strength between SSM and deeper RZSM was stronger in dry regions (northwest) than that in wet regions (southeast), which confirmed the results in Nebraska but contrasted with that of Oklahoma reported by Ford et al. [40]. As mentioned above, the soil moisture

might affect the patterns of precipitation by controlling the evapotranspiration and other energy fluxes. Boé et al. [17] indicated that the precipitation tended to be larger in dry soil conditions. Taylor et al. [55] also found that the afternoon precipitation preferentially fell over dry soil regions where convective events driven by increased sensible heat flux over dry soil occurred frequently. Thus, the negative correlation between precipitation and coupling strength could be explained by the negative soil moisture–precipitation feedback caused by the specific circulation regime or convective events.

The right panel of Figure 4 shows similar characteristics but for maximum cross correlation coefficient and average annual air temperature (°C). There was a negative correlation between air temperature and soil moisture coupling strength of 5–20 cm (R^2 = 0.18), 5–40 cm (R^2 = 0.26) and 5–100 cm (R^2 = 0.33), respectively. The difference is that the coefficient of determination (R^2) associated with air temperature was constantly lower than precipitation at different depths, which showed that precipitation might have a stronger control on coupling strength between SSM and RZSM than air temperature. One reason for the negative correlation between coupling strength and air temperature could be explained as follows: The net radiation heat was partitioned into latent heat flux for evapotranspiration and sensible heat flux for rising air temperature. Therefore, the latent heat flux consumed by dry soil was less than wet soil; the remaining sensible heat flux for dry soil was more than wet soil, which increased air temperature [56–58]. In addition, the hydraulic connection and coupling strength of dry soil is weaker than wet soil, so the maximum cross-coefficient and air temperature is negatively correlated. Finally, due to the strong land surface–atmosphere interactions, precipitation and air temperature might have stronger effect on the coupling strength for 5–20 cm soil moisture than 5–40 cm and 5–100 cm soil moisture, so R^2 increased with soil depth.

The cross-correlation analysis above implied that SSM had a strong connection with the RZSM over in situ stations in HRB. Similar results were reported by [24,25]. Thus, it is promising to establish links between SSM and RZSM. However, there are obvious outliers in the scatterplots for Figure 4a,b. First, these in situ stations are mostly located in or close to the mountainous regions of the HRB (e.g., northeast, southwest and northwest of the HRB), where the underlying surface and local weather conditions are different from that in the plain region. Thus, these differences result in heat and moisture exchange between land surface and atmosphere distinctly different in mountainous and plain regions, respectively. In general, the underlying surface in mountainous regions is more complex than that in plain regions, which impedes the transfer and exchange of heat and moisture in the vadose zone, and further weakens the response of coupling strength to precipitation or air temperature. Moreover, due to the stronger land–atmosphere interactions in the surface layer than the root zone layer, the mixed effect of precipitation and air temperature on the coupling strength for 5–20 cm soil moisture leads to the low correlation coefficient between the coupling strength and precipitation or air temperature, i.e., the coupling strength for 5–20 cm soil moisture is not dominated by sole precipitation or air temperature.

3.3. Analysis of T_{opt}

In the study, SWI_o at 5 cm was used to predict SWI_m at 20, 40, 100 cm and profile average values at the in situ stations. Figure 5 shows that NSE between SWI_o and SWI_m at different depths varied with time for each station. The station-specific T_{opt} was obtained when the NSE peaked. The statistics of T_{opt} at different depth and evaluation metrics are presented in Table 1. For the HRB stations, the T_{opt} ranged from 1 to 25 days with an average value of 4 days at 20 cm, from 1 to 60 days with an average value of 8 days at 40 cm, from 2 to 60 days with an average value of 36 days at 100 cm, and from 1 to 60 days with an average value of 11 days for the profile average value. The T_{opt} at 20 cm was smaller than results from Wagner et al. [34] and Wang et al. [41], who used SWI_o at 5 cm to predict SWI_m at 20 cm with T_{opt} = 15 and 15.8 days, respectively. The T_{opt} at 40 cm was also smaller than previous results. For instance, Albergel et al. [33] used SWI_o at 5 cm to estimate SWI_m at 30 cm in SMOSMANIA and SMOSREX networks by setting T_{opt} = 6 days, and Tian et al. [2]

used SWI_o at 5 cm to predict SWI_m at 40 cm with T_{opt} = 12.4 days. By contrast, The T_{opt} at 100 cm was also larger than the results reported by Wagner et al. [34], who used SWI_o at 5 cm to estimate the SWI_m at 100 cm with T_{opt} = 20 days. The reasoning can be explained as follows: the soil column is divided into the plough layer (0–20 cm), black soil layer (20~50 cm) and the lime concretion soil layer (50~100 cm) due to the soil stratification in the HRB, so the relative impervious layer hinders the infiltration of soil water and hence results in a larger T_{opt} at 100 cm [59]. Table 1 also lists the statistics of T_{opt} using surface SWI_o to predict root zone SWI_m and corresponding NSE reported in the previous literature. Overall, T_{opt} tended to increase and NSE tended to decrease with soil depth.
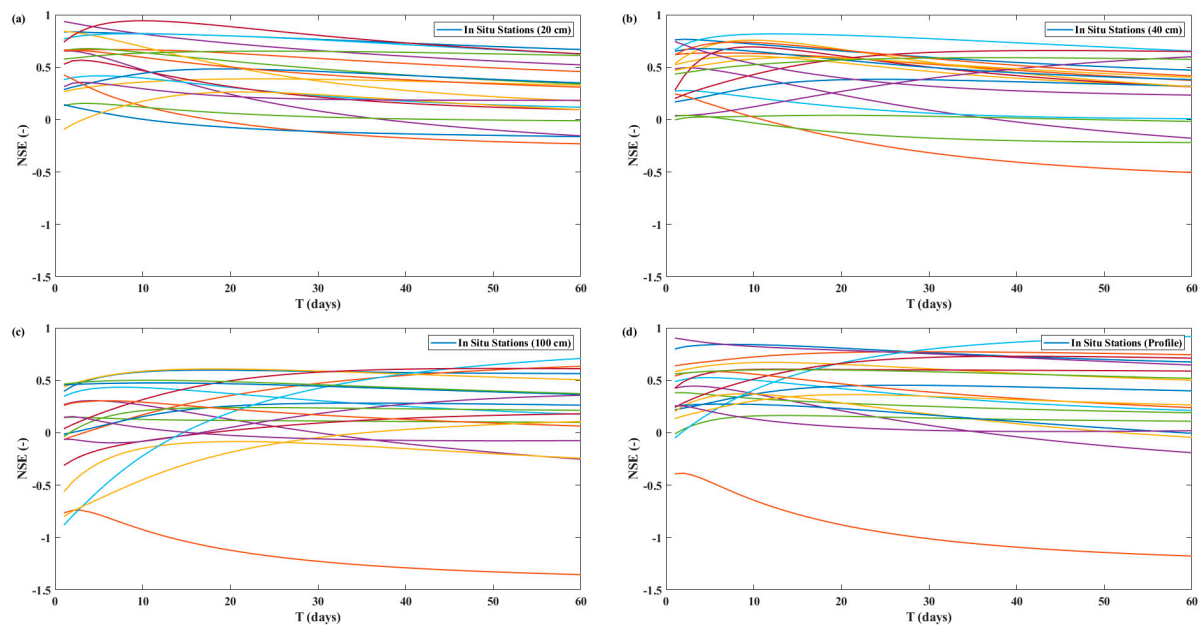
Figure 5. NSE between SWI_o and SWI_m at the depths of 20 (**a**), 40 (**b**), 100 cm (**c**) and for the profile average value (**d**). SWI_o standardized by daily volumetric soil moisture at the depth of 5 cm is used to estimated SWI_m at the depths of 20 cm, 40 cm, 100 cm and for the profile average value. Each color represents a station.

Table 1. Statistics of the characteristic time length T_{opt} using near-surface SWI to predict SWI at various root zone depths and corresponding NSE values.

Source	Depth	T_{opt} (Days)	Mean of T_{opt}	NSE	Mean of NSE
This article (5 cm)	20 cm	1–25	4	0.14–0.94	0.57
	40 cm	1–60	8	0.04–0.82	0.55
	100 cm	2–60	36	−0.74–0.71	0.31
	soil profile	1–60	11	−0.39–0.92	0.50
[2] (5 cm)	15 cm	1–6	2.48	0.27–0.99	0.63
	25 cm	1–24	7.29	−0.09–0.91	0.41
	40 cm	1–48	12.37	−0.23–0.71	0.24
	60 cm	1–60	18.93	−0.64–0.64	−0.03
	soil profile	1–11	4.32	0.32–0.96	0.64

Table 1. *Cont.*

Source	Depth	T_{opt} (Days)	Mean of T_{opt}	NSE	Mean of NSE
(10 cm) [41] (5 cm)	25 cm	2–58	10.47	0.03–0.86	0.59
	50 cm	4–60	29.78	−1.24–0.68	0.24
	soil profile	1–22	4.81	0.33–0.91	0.76
	10 cm	1–60	4.90	−3.57–0.94	0.57
	20 cm	1–60	15.83	−6.66–0.92	0.05
	50 cm	1–60	31.71	−5.86–0.77	−0.50
	soil profile	1–60	9.98	−3.58–0.91	0.42
[40] (5 and 10 cm)	25 cm	2–22	8	0.07–0.84	0.63
	25 cm	3–20	9	0.08–0.83	0.64
[33] (5 cm)	30 cm	3–11	6	0.56–0.94	0.85
[60] (5 cm)	25 cm	20–60	40	0.62–0.77	0.67
	(50~100) cm	50–60	60	0.41–0.74	0.62
	100 cm	40–60	50	0.57–0.75	0.69
[34] (5 cm)	20 cm	15–30	15	/	/
	100 cm	15–30	20	/	/

T_{opt} varied considerably over different in situ stations. In order to apply the exponential filter on large spatial scale, so we evaluated the performance of the exponential filter using the stations-averaged T_{opt} and precipitation-based T_{pre} for specific depth. Figure 6 shows boxplot of NSE, RMSE and MBE between SWI_o and SWI_m for two different T_{opt}. The NSE first increased with T, then decreased to a steady value when the T reached 60 days. For stations-averaged T_{opt}, the NSE ranged from 0.03 to 0.89 with an average value of 0.53 at 20 cm, from −0.01 to 0.81 with an average value of 0.46 at 40 cm, from −1.26 to 0.60 with an average value of 0.19 at 100 cm, and from −0.67 to 0.84 with an average value of 0.42 for the profile average value. The NSE, at depth of 20 cm was larger than that of 40, 100 cm and profile average value, which was consistent with the trend of coupling strength between SSM and RZSM. For precipitation-based T_{pre}, the NSE between SWI_o and SWI_m ranged from 0.37 to 0.94 with an average value of 0.63 at 20 cm, from 0.24 to 0.82 with an average value of 0.59 at 40 cm, from −0.74 to 0.71 with an average value of 0.32 at 100 cm, and from −0.38 to 0.84 with an average value of 0.55 for the profile average value. On the whole, the precipitation-based T_{pre} outperformed stations-averaged T_{opt}. A summary of the statistical metrics is shown in Table 2.

3.4. Controlling Factors on T_{opt}

The characteristic time length T_{opt} is the unique variable of the exponential filter, so it is pivotal to figuring out that variables mainly control the T_{opt}, which reflects the time scale of soil moisture dynamics. Soil depth, soil properties (bulk density, clay/sand/silt fraction, soil organic matter and porosity) and precipitation are used to investigate how T_{opt} is affected. Figure 7 shows the boxplot of T_{opt} at depths of 20, 40, 100 cm and the profile average value over all in situ stations. We are confident it infers that T_{opt} tends to increase with soil depth. The stations-averaged T_{opt} are 4, 8, 36 and 11 days, respectively. No significant correlation was found between soil properties and T_{opt} (Figure S1), so it was not shown here.
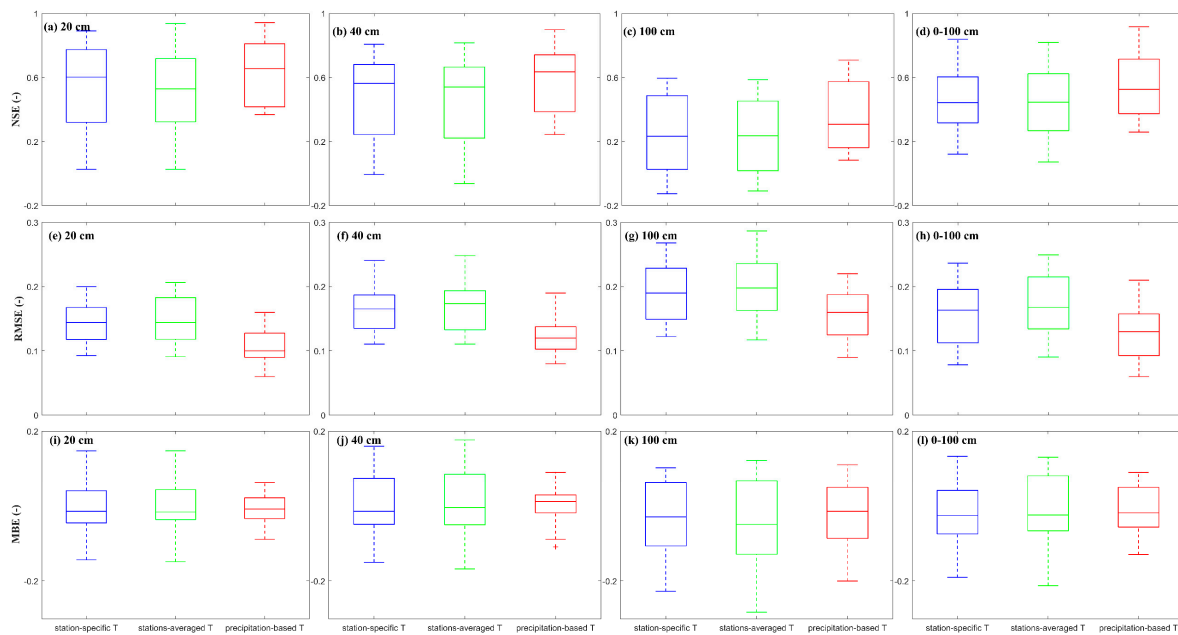
Figure 6. Box plots of NSE (**a**–**d**), RMSE (**e**–**h**) and MBE (**i**–**l**) at depths of 20 cm, 40 cm, 100 cm and for the profile average value for the station-specific T, stations-averaged T and precipitation-based T.

Table 2. Statistical metrics of NSE, RMSE and MBE at depths of 20, 40, 100 cm and profile average value, calculated with observed SWI_o standardized by daily volumetric soil moisture and predicted SWI_m from normalized near-surface soil moisture with the exponential filter.

			NSE		RMSE		MBE	
Depth	**Statics**	T_{opt} **(Days)**	**Stations-Averaged T**	**Precipitation-Based T**	**Stations-Averaged T**	**Precipitation-Based T**	**Stations-Averaged T**	**Precipitation-Based T**
20 cm	Range	1–25	0.03–0.89	0.37–0.94	0.10–0.21	0.06–0.16	−0.15–0.15	−0.09–0.06
	Average	4	0.53	0.63	0.15	0.11	0.00	0.00
	SD	8.26	0.27	0.2	0.04	0.03	0.07	0.04
40 cm	Range	1–60	−0.01–0.81	0.24–0.82	0.11–0.25	0.08–0.16	−0.16–0.17	−0.11–0.09
	Average	8	0.46	0.59	0.17	0.12	0.01	0.00
	SD	16.44	0.29	0.24	0.04	0.03	0.09	0.05
100 cm	Range	2–60	−1.26–0.6	−0.74–0.71	0.12–0.29	0.09–0.22	−0.28–0.12	−0.19–0.11
	Average	36	0.19	0.32	0.20	0.16	−0.04	−0.03
	SD	23.62	0.42	0.32	0.05	0.04	0.12	0.09
Profile	Range	1–60	−0.67–0.84	−0.38–0.84	0.10–0.25	0.08–0.21	−0.21–0.13	−0.13–0.09
	Average	11	0.42	0.55	0.17	0.13	−0.01	−0.01
	SD	15.71	0.33	0.22	0.05	0.04	0.10	0.06

Precipitation is the most important driver for soil moisture variation. Figure 8 shows that T_{opt} was negatively correlated with average annual precipitation at all depths. The coefficients of determination (R^2) between T_{opt} and average annual precipitation were ($R^2 = 0.37$) at 20 cm, ($R^2 = 0.33$) at 40 cm, ($R^2 = 0.30$) at 100 cm and ($R^2 = 0.31$) for profile average value. The quantitative analysis between T_{opt} and precipitation helps us better comprehend how soil moisture and precipitation participate in land–atmosphere interactions and affect each other. There is a feedback mechanism (positive or negative) between soil moisture and precipitation, which contributes to predicate droughts and floods from the soil moisture [18,19,55]. For in situ stations with higher precipitation, the hydraulic connection between near-surface and root zone soil water was enhanced due to the frequent precipitation, which improved the infiltration rate for soil water and provided faster

drainage conditions. Therefore, a smaller T_{opt} was found for in situ stations with higher precipitation. The abnormally large T_{opt} values mainly exist in the mountainous regions or north of the HRB with less precipitation. For the in situ stations in the mountainous regions, the precipitation reaches the land surface quickly form surface runoff due to the effect of topography (e.g., steep slope), and less precipitation infiltrates into the soil. In addition, the water infiltrating into the soil may be hindered by the relatively impermeable layer (rock formation) and form subsurface runoff. Both reduce the response of T_{opt} value to precipitation. For the in situ stations in the northern HRB, which commonly has less precipitation than that in the southern and eastern HRB bordering the Yellow Sea due to the geographic location. Therefore, less precipitation reaches the land surface and infiltrate into the vadose zone, which takes more time from surface layer to root zone layer, thus producing a large T_{opt} value.
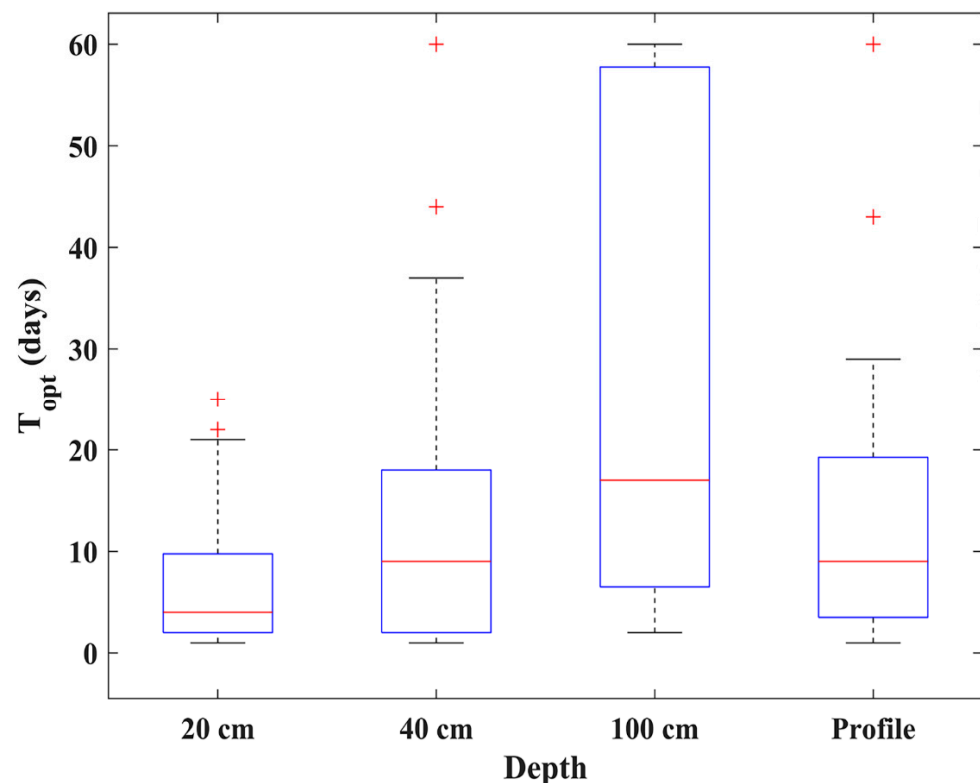
Figure 7. Boxplot of T_{opt} at the depths of 20, 40, 100 cm and for the profile average value for the station-specific T_{opt}. "+" represent outliers of T_{opt}. The T_{opt} represented by each boxplot is divided into six parts by the minimum value, lower quartile (25th percentile), median (50th percentile), upper quartile (75th percentile), maximum value, respectively.

3.5. Evaluation of RF_SMAP_L3_P SSM Product

The in situ SSM was used to validate the reconstructed RF_SMAP_L3_P SSM, SMAP L4 SSM and SMOS L3 SSM from 2015 to 2019. Evaluation metrics of R, Bias, RMSE and ubRMSE were used to evaluate the accuracy of specific SSM products. Figure 9 (left) displays the SSM time series of model products and in situ measurements. On the whole, there was a significant underestimation of SSM by the SMOS L3 product, but for days with high precipitation, the SMOS L3 product overestimated in situ SSM. SMAP L4 SSM significantly overestimated the in situ measurements when precipitation was low. Figure 9 (right) shows the scatterplots between model SSM and in situ measurements. RF_SMAP_L3_P SSM had the highest R of 0.63, followed by SMAP L4 SSM (R = 0.608) and SMOS L3 (R = 0.445). SMAP L4 SSM had the lowest ubRMSE of 0.032, followed by RF_SMAP_L3_P SSM (ubRMSE = 0.040), and both satisfied the accuracy requirement of 0.04 (m^3/m^3). SMOS L3 had ubRMSE = 0.046. Compared to other model products, the

reconstructed RF_SMAP_L3_P SSM best captured the temporal variations of in situ soil moisture and had the lowest MBE. Although RF_SMAP_L3_P had a higher ubRMSE than that of SMAP L4 SSM, we think that it could be used as the exponential filter input to estimate RZSM at different depths.
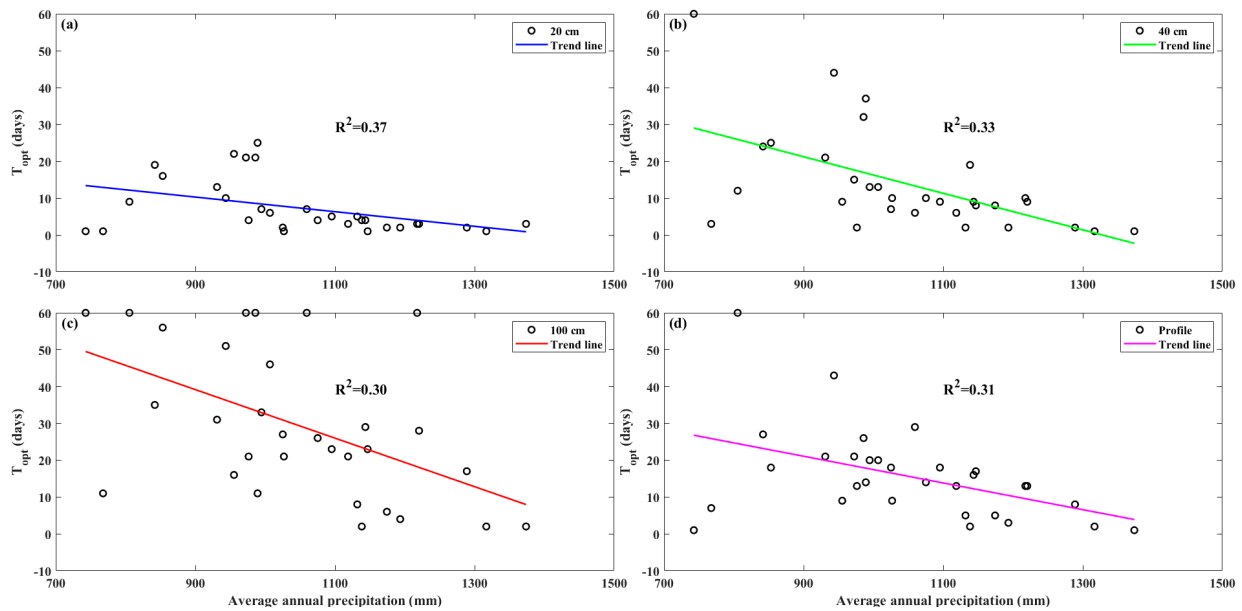
Figure 8. Scatter plots between T_{opt} and average annual precipitation over all stations at depths of 20 (**a**), 40 (**b**), 100 (**c**) and profile average value (**d**), each circle represents a soil moisture station, color lines represent the trends of the scattered points.
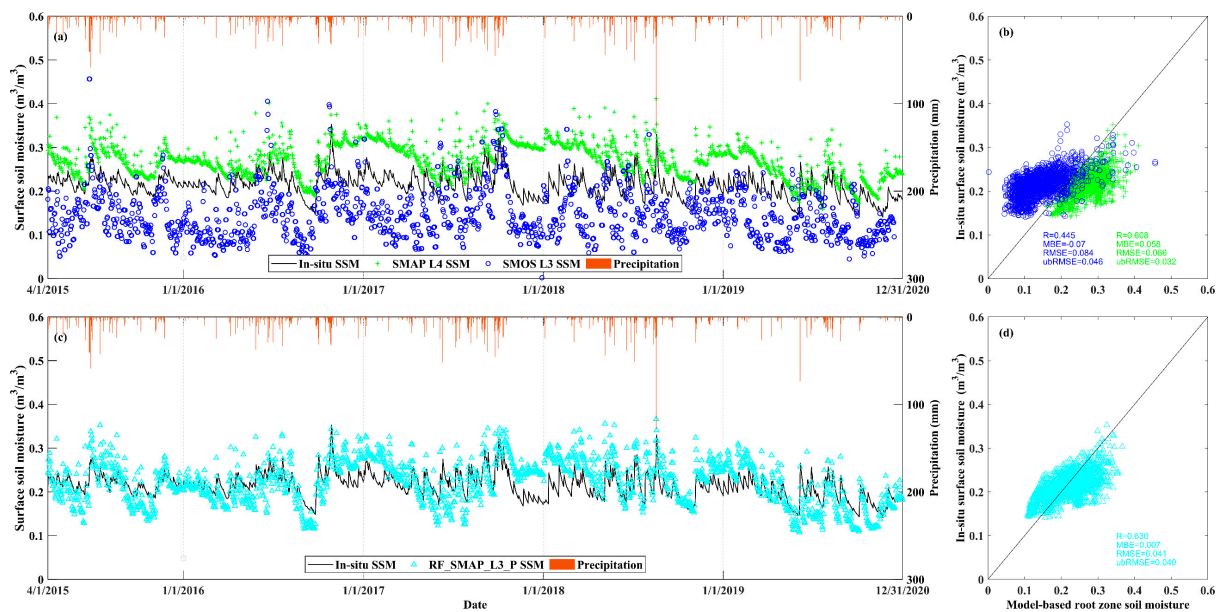
Figure 9. Left panel (**a**,**c**) shows the time series comparison between in situ SSM and model products (SMAP L4 and SMOS L3 SSM); right panel (**b**,**d**) is the scatterplots. Blue circle represents SMOS L3 SSM; green cross represents SMAP L4 SSM; cyan triangle represents RF_SMAP_L3_P SSM.

3.6. Estimation and Evaluation of RZSM from RF_SMAP_L3_P SSM

The scaled RF-SMAP_L3_P SSM (0–5 cm) was adopted to estimate root zone SWI (20 cm, 40 cm, 100 cm and 0–100 cm) using the exponential filter method from 2015 to 2019, the precipitation-based T_{pre} ($T_{pre} = 4$ at 20 cm, 8 at 40 cm, 36 at 100 cm, 11 at 0–100 cm)

were considered as the unique parameter to participate the calculation of root zone SWI, then root zone SWI was rescaled linearly to volumetric soil moisture, which was used to compare to in situ volumetric soil moisture.

Figure 10 displays the stations-averaged time series and scatterplots of RZSM at different depths, generally speaking, the accuracy of RZSM estimates decreased with soil depth, which was consistent with coupling strength. The evaluation metrics of R were 0.554, 0.500 and 0.290; those of MBE were −0.022, −0.025 and −0.064; and of RMSE were 0.038, 0.039 and 0.071 at depths of 20, 40 and 100 cm, respectively. However, the ubRMSE decreased with soil depth, probably because the bias increased faster than RMSE with soil depth. In general, compared to in situ RZSM, the RZSM estimates at all depths derived from the exponential filter were lower.
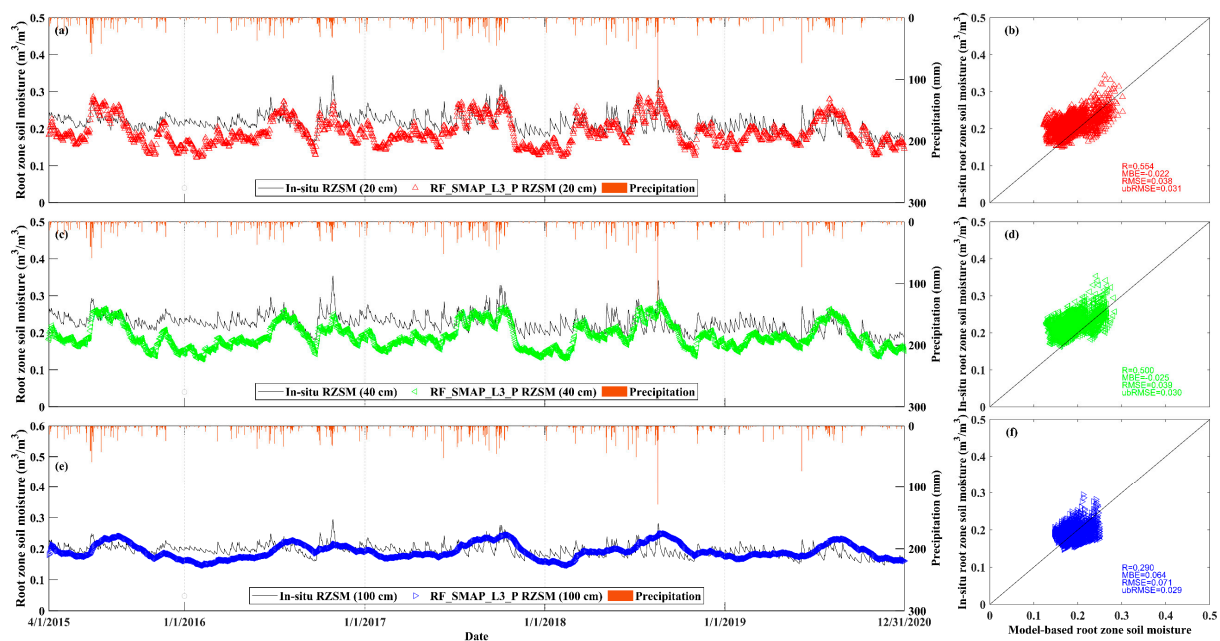
Figure 10. Left panel (**a**,**c**,**e**) shows the time series comparison between in situ RZSM and RF_SMAP_L3_P RZSM at depths of 20, 40 and 100 cm; right panel (**b**,**d**,**f**) is for the scatterplot.

Figure 11 shows the boxplots of evaluation metrics over all in situ stations. Generally speaking, the accuracy of RZSM estimates decreased with soil depth. The evaluation metric of R ranged from 0.19 to 0.59 with an average value of 0.40 at depth of 20 cm, from 0 to 0.54 with an average value of 0.35 at depth of 40 cm, from −0.15 to 0.39 with an average value of 0.20 at depth of 100 cm. The average ubRMSE was 0.045 at 20 cm (ranging from 0.033 to 0.069), 0.046 at 40 cm (from 0.032 to 0.075), 0.041 at 100 cm (from 0.021 to 0.068). Table 3 provides a summary of evaluation metrics.

In this section, we evaluated the accuracy of RF_SMAP_L3_P RZSM, SMAP L4 RZSM and SMOS L4 RZSM compared to in situ RZSM. The left panel of Figure 12 shows the time series comparison between in situ RZSM and model products, the right panel of Figure 12 are scatterplots. RF_SMAP_L3_P RZSM had the highest R of 0.586, followed by SMAP L4 SSM (R = 0.540) and SMOS L3 (R = 0.359), and the lowest ubRMSE of 0.023, followed by RF_SMAP_L3_P SSM (ubRMSE = 0.027) and SMOS L3 (ubRMSE = 0.027), all of them satisfied the accuracy requirement of 0.04 (m^3/m^3). There was no doubt that the R and ubRMSE for RZSM was lower than that for SSM, which was consistent with the conclusion drown by Reichle et al. [61]. In general, all model products could roughly reproduce the in situ RZSM. It was clear that the SMOS L4 RZSM was constantly lower than in situ measurements, which was similar to the SMOS L3 SSM, and it didn't respond very well to precipitation. The underestimation of SMOS L4 SSM might be explained by the following two reasons. Firstly, SMOS L3 SSM underestimated the in situ measurements.

Secondly, the root zone SWI derived from exponential filter was lower than that of the in situ measurements. SMAP L4 and RF_SMAP_L3_P RZSM both captured the temporal variation of RZSM better than SMOS L4 RZSM; both of them matched the high in situ measurements well, but slightly overestimated the low in situ measurements. In conclusion, though showing slightly higher MBE (0.04) and RMSE (0.046) of RF_SMAP_L3_P RZSM than SMAP L4 RZSM (MBE = 0.030, RMSE = 0.046), RF_SMAP_L3_P RZSM had the highest R and the lowest ubRMSE (<0.04 m^3/m^3) among all RZSM products; we believe that RF_SMAP_L3_P RZSM captured the temporal variation of in situ measurements best.
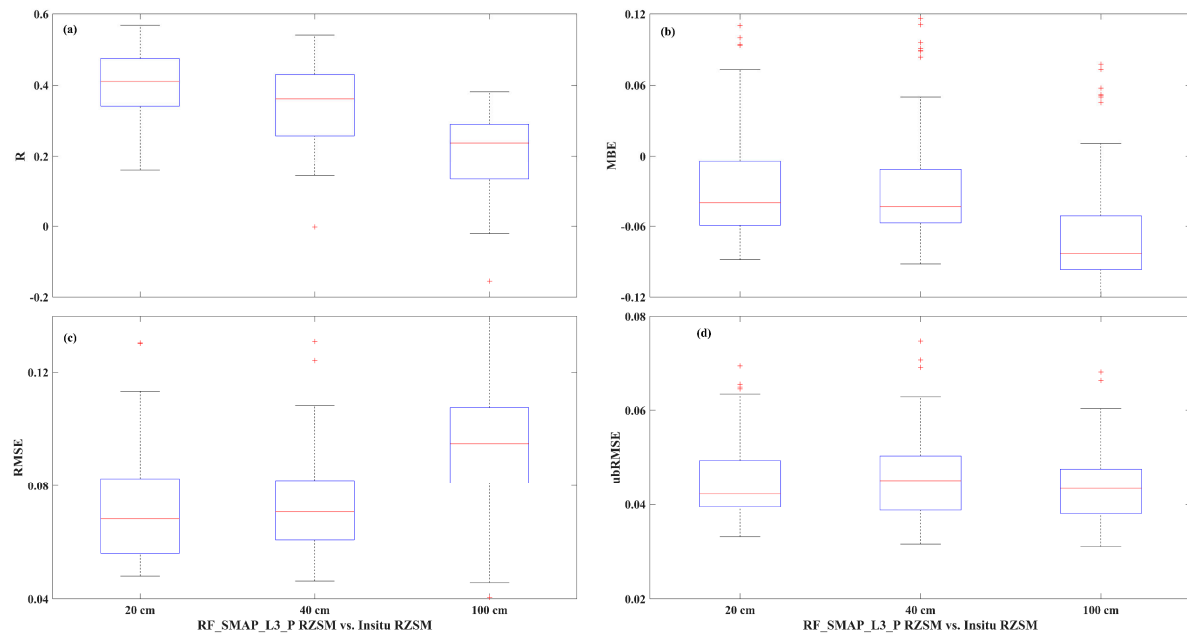
Figure 11. The evaluation metrics of R (**a**), MBE (**b**), RMSE (**c**) and ubRMSE (**d**) at the depths of 20, 40, 100 cm between SWI_o normalized by in situ soil moisture and SWI_m estimated by RF_SMAP_P_L3 surface soil moisture. "+" represent outliers of T_{opt}.

Table 3. Summary of metrics (R, MBE, RMSE and ubRMSE) between estimated SWI_m and observed SWI_o at depths of 20, 40 and 100 cm.

Depth	Statistics	R	MBE	RMSE	ubRMSE
20 cm	Range	0.19–0.59	−0.08–0.02	0.08–0.13	0.03–0.07
	Mean	0.40	−0.02	0.07	0.04
40 cm	Range	0–0.54	−0.11–0.11	0.05–0.13	0.03–0.07
	Mean	0.35	−0.03	0.08	0.05
100 cm	Range	−0.15–0.39	−0.13–0.32	0.04–0.33	0.02–0.07
	Mean	0.20	0	0.12	0.04

Because floods and droughts occurred frequently in the Huai River Basin, we divided the research period into a flood period (May–September) and non-flood period (October–April) to investigate the performance of different RZSM products. Figure 13 displays the boxplots of R, MBE, RMSE and ubRMSE between in situ RZSM and model RZSM products over all in situ stations. RF_SMAP_L3_P RZSM obtained the highest R mean and lowest ubRMSE mean than the other products, followed by SMAP L4 RZSM. SMOS L4 RZSM performed worse than the former due to a lower R mean and higher ubRMSE mean, and the negative bias SMOS L4 RZSM indicated that it underestimated the subsurface soil moisture. All the evaluation metrics of SMAP L4 and RF_SMAP_L3_P RZSM in the flood period had better performance than that of the full period and non-flood period. In the flood period, the average R value was 0.564 with an SD of 0.101 for RF_SMAP_L3_P, 0.470

with an SD of 0.104 for SMAP. The average ubRMSE value was 0.033 with an SD of 0.007 for RF_SMAP_L3_P, 0.039 with an SD of 0.008. By comparison, among three research periods, SMOS L4 RZSM performed better in the non-flood period. In the non-flood period, the average R value for SMOS L4 RZSM was 0.200 with an SD of 0.167, and the average ubRMSE value was 0.037 with an SD of 0.007. For SMOS L4 RZSM, though the R of the non-flood period was higher than that of flood period, the same went for the SD, which might be caused by temporally uneven precipitation in the non-flood period.
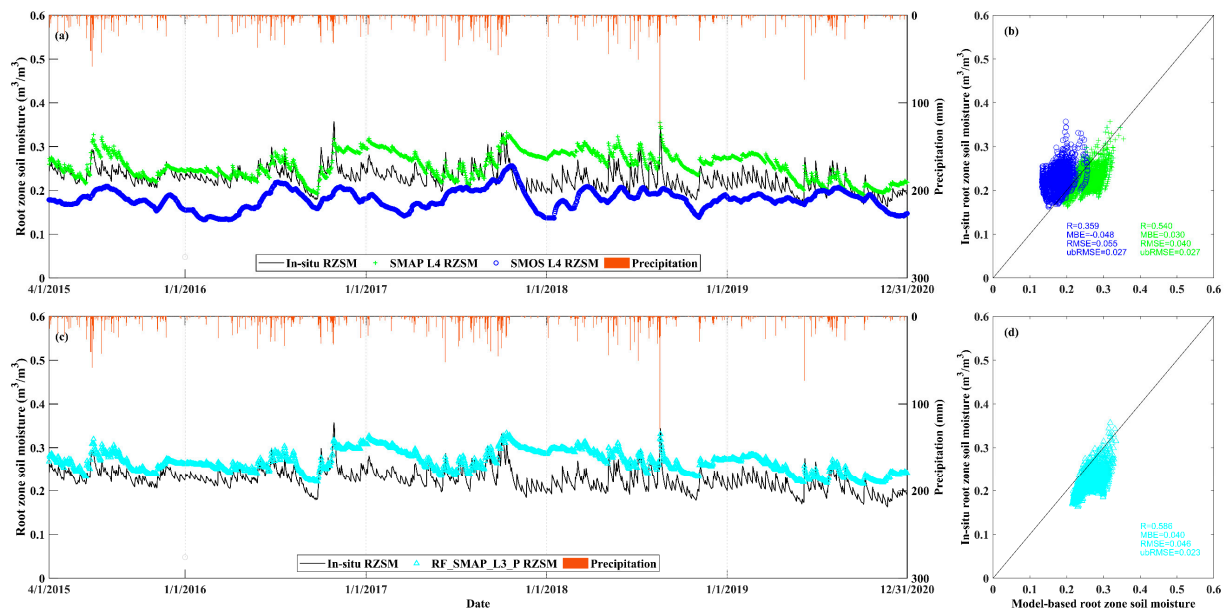
Figure 12. Same as Figure 9, but for the RZSM (0–100 cm). Left panel (**a**,**c**) shows the time series of in situ observations and RZSM model products. Right panel (**b**,**d**) shows the scatterplot.
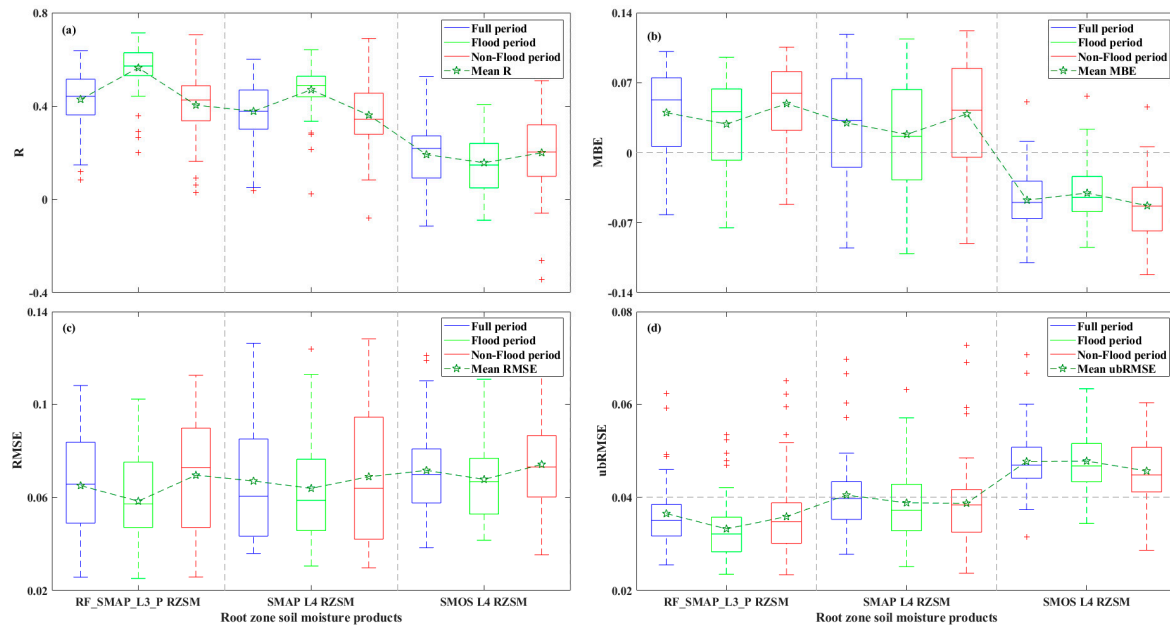
Figure 13. Boxplots of evaluation metrics (R: (**a**); MBE: (**b**); RMSE: (**c**); ubRMSE: (**d**)) between model RZSM and in situ measurements in different periods. "+" represent outliers of T_{opt}.

4. Conclusions

In this study, we assessed the utility of the recursive exponential filter method using in situ soil moisture measurements from 2015 to 2019 in the HRB. In addition, the impact of controlling factors on the unique parameter T_{opt} was investigated. The filter method was applied at a watershed scale by using a new RF_SMAP_L3_P soil moisture dataset (0–5 cm) to estimate RF_SMAP_L3_P RZSM over the Huai River Basin. Finally, we evaluated the performance of RF_SMAP_L3_P RZSM with SMAP L4 and SMOS L4 RZSM. The main findings were as follows:

(1) The coupling strength between SSM and RZSM was strong and correlated negatively with precipitation and air temperature for the pivotal role of soil moisture in land–atmosphere interactions.

(2) There exists a hysteresis pattern between CV of spatial soil moisture and mean spatial soil moisture. The root zone soil moisture leads to a slight increase in the occurrence of hysteresis comparing with surface soil moisture. In general, a low precipitation event would mask the hysteresis pattern comparing with a high precipitation event.

(3) The ExpF could be used to estimate RZSM from SSM (satellite-derived or model data) with reasonable accuracy at the watershed scale, but its utility declined with soil depth. And it performed better in wetter weather conditions than dry weather conditions. Precipitation-based T_{pre} significantly improved the accuracy of the exponential filter at a basin scale when it was applied to grid units, but it was subject to the accuracy of precipitation. However, gridded precipitation used to obtain T_{pre} was generally provided by reanalysis products or satellite-based retrievals, which had relatively large uncertainty to gauge-based observations and affected the acquisition of accurate T_{pre} in this study.

(4) The ExpF might not be suitable for application in mountainous regions. Steep slope is more conductive to the quick formation of surface runoff than flat plain and less precipitation infiltrates into the soil. In addition, the water infiltrating into the soil could be hindered by the relatively impermeable layer (rock formation) and form subsurface runoff. Both mentioned above reduce the response of transfer of water in the soil to precipitation.

(5) Among the three research periods, RF_SMAP_L3_P and SMAP L4 RZSM had better performance during the flood period, but SMOS L4 RZSM performed better in the non-flood period. Among all of the RZSM products, RF_SMAP_L3_P RZSM captured the temporal variation of in situ soil moisture best and SMAP L4 RZSM had the lowest MBE.

References

1. Legates, D.R.; Mahmood, R.; Levia, D.F.; DeLiberty, T.L.; Quiring, S.M.; Houser, C.; Nelson, F.E. Soil moisture: A central and unifying theme in physical geography. *Prog. Phys. Geogr.* **2010**, *35*, 65–86. [CrossRef]
2. Tian, J.; Han, Z.; Bogena, H.R.; Huisman, J.A.; He, C. Estimation of subsurface soil moisture from surface soil moisture in cold mountainous areas. *Hydrol. Earth Syst. Sci. Discuss.* **2020**, *24*, 4659–4674. [CrossRef]
3. Alemohammad, S.H.; Kolassa, J.; Prigent, C.; Aires, F.; Gentine, P. Global Downscaling of Remotely-Sensed Soil Moisture using Neural Networks. *Hydrol. Earth Syst. Sci. Discuss.* **2018**, *22*, 5341–5356. [CrossRef]
4. Babaeian, E.; Sadeghi, M.; Jones, S.B.; Montzka, C.; Vereecken, H.; Tuller, M. Ground, Proximal, and Satellite Remote Sensing of Soil Moisture. *Rev. Geophys.* **2019**, *57*, 530–616. [CrossRef]
5. Dobriyal, P.; Qureshi, A.; Badola, R.; Hussain, S.A. A review of the methods available for estimating soil moisture and its implications for water resource management. *J. Hydrol.* **2012**, *458*, 110–117. [CrossRef]
6. Brocca, L.; Melone, F.; Moramarco, T.; Wagner, W.; Naeimi, V.; Bartalis, Z.; Hasenauer, S. Improving runoff prediction through the assimilation of the ASCAT soil moisture product. *Hydrol. Earth Syst. Sci.* **2010**, *14*, 1881–1893. [CrossRef]
7. Brocca, L.; Melone, F.; Moramarco, T. Soil Moisture Monitoring at Different Scales for Rainfall-Runoff Modelling. In Proceedings of the 4th International Congress on Environmental Modelling and Software, Barcelona, Spain, 7–10 July 2008; pp. 407–414. Available online: http://scholarsarchive.byu.edu/iemssconference/2008/all/63 (accessed on 1 January 2023).
8. Srivastava, A.; Saco, P.M.; Rodriguez, J.F.; Kumari, N.; Chun, K.P.; Yetemen, O. The role of landscape morphology on soil moisture variability in semi-arid ecosystems. *Hydrol. Process.* **2020**, *35*, e13990. [CrossRef]
9. Teuling, A.J.; Hupet, F.; Uijlenhoet, R.; Troch, P.A. Climate variability effects on spatial soil moisture dynamics. *Geophys. Res. Lett.* **2007**, *34*, L06406. [CrossRef]
10. Fatichi, S.; Katul, G.G.; Ivanov, V.Y.; Pappas, C.; Paschalis, A.; Consolo, A.; Kim, J.; Burlando, P. Abiotic and biotic controls of soil moisture spatiotemporal variability and the occurrence of hysteresis. *Water Resour. Res.* **2015**, *51*, 3505–3524. [CrossRef]
11. Tobin, K.J.; Crow, W.T.; Dong, J.; Bennett, M.E. Validation of a New Root-Zone Soil Moisture Product: Soil MERGE. *IEEE J. Sel. Top. Appl. Earth Obs. Remote Sens.* **2019**, *12*, 3351–3365. [CrossRef]
12. Collow, T.W.; Robock, A.; Basara, J.B.; Illston, B.G. Evaluation of SMOS retrievals of soil moisture over the central United States with currently available in situ observations. *J. Geophys. Res. Atmos.* **2012**, *117*, D09113. [CrossRef]
13. Pablos, M.; González-Zamora, Á.; Sánchez, N.; Martínez-Fernández, J. Assessment of Root Zone Soil Moisture Estimations from SMAP, SMOS and MODIS Observations. *Remote Sens.* **2018**, *10*, 981. [CrossRef]
14. Abolafia-Rosenzweig, R.; Livneh, B.; Small, E.E.; Kumar, S.V. Soil Moisture Data Assimilation to Estimate Irrigation Water Use. *J. Adv. Model. Earth. Syst.* **2019**, *11*, 3670–3690. [CrossRef]
15. Jalilvand, E.; Abolafia-Rosenzweig, R.; Tajrishy, M.; Das, N. Evaluation of SMAP/Sentinel 1 High-Resolution Soil Moisture Data to Detect Irrigation Over Agricultural Domain. *IEEE J. Sel. Top. Appl. Earth Obs. Remote Sens.* **2021**, *14*, 10733–10747. [CrossRef]
16. Brocca, L.; Ciabatta, L.; Massari, C.; Moramarco, T.; Hahn, S.; Hasenauer, S.; Kidd, R.; Dorigo, W.; Wagner, W.; Levizzani, V. Soil as a natural rain gauge: Estimating global rainfall from satellite soil moisture data. *J. Geophys. Res. Atmos.* **2014**, *119*, 5128–5141. [CrossRef]
17. Boé, J. Modulation of soil moisture–precipitation interactions over France by large scale circulation. *Clim. Dyn.* **2012**, *40*, 875–892. [CrossRef]
18. McColl, K.A.; Alemohammad, S.H.; Akbar, R.; Konings, A.G.; Yueh, S.; Entekhabi, D. The global distribution and dynamics of surface soil moisture. *Nat. Geosci.* **2017**, *10*, 100–104. [CrossRef]
19. Tuttle, S.; Salvucci, G. Empirical evidence of contrasting soil moisture-precipitation feedbacks across the United States. *Science* **2016**, *352*, 825–828. [CrossRef]
20. Kędzior, M.; Zawadzki, J. SMOS data as a source of the agricultural drought information: Case study of the Vistula catchment, Poland. *Geoderma* **2017**, *306*, 167–182. [CrossRef]
21. Baldwin, D.; Manfreda, S.; Keller, K.; Smithwick, E.A.H. Predicting root zone soil moisture with soil properties and satellite near-surface moisture data across the conterminous United States. *J. Hydrol.* **2017**, *546*, 393–404. [CrossRef]
22. Mahmood, R.; Hubbard, K.G. Relationship between soil moisture of near surface and multiple depths of the root zone under heterogeneous land uses and varying hydroclimatic conditions. *Hydrol. Process.* **2007**, *21*, 3449–3462. [CrossRef]
23. Calvet, J.C.; Noilhan, J. From Near-Surface to Root-Zone Soil Moisture Using Year-Round Data. *J. Hydrometeorol.* **2000**, *1*, 393–411. [CrossRef]
24. Martinez, C.; Hancock, G.R.; Kalma, J.D.; Wells, T. Spatio-temporal distribution of near-surface and root zone soil moisture at the catchment scale. *Hydrol. Process.* **2008**, *22*, 2699–2714. [CrossRef]

25. Mahmood, R.; Littell, A.; Hubbard, K.G.; You, J. Observed data-based assessment of relationships among soil moisture at various depths, precipitation, and temperature. *Appl. Geogr.* **2012**, *34*, 255–264. [CrossRef]

26. Camps, A.; Gourrion, J.; Tarongi, J.M.; Vall Llossera, M.; Gutierrez, A.; Barbosa, J.; Castro, R. Radio-Frequency Interference Detection and Mitigation Algorithms for Synthetic Aperture Radiometers. *Algorithms* **2011**, *4*, 155–182. [CrossRef]

27. Wang, X.; Lü, H.; Crow, W.; Zhu, Y.; Wang, Q.; Su, J.; Zheng, J.; Gou, Q.; Wang, X.; Liu, E. Potential Feasibility of NASA-derived products in Filling SMAP Soil Moisture Gaps by Random Forest: A case in a humid and sub-humid basin. *J. Hydrol.* **2022**, *under review*. Available online: https://pan.baidu.com/s/1AYM1EcmiBvLOAfXZQae1LQ?pwd=od5m (accessed on 1 January 2023).

28. Gao, X.; Zhao, X.; Brocca, L.; Pan, D.; Wu, P. Testing of observation operators designed to estimate profile soil moisture from surface measurements. *Hydrol. Process.* **2019**, *33*, 575–584. [CrossRef]

29. Zhang, N.; Quiring, S.; Ochsner, T.; Ford, T. Comparison of Three Methods for Vertical Extrapolation of Soil Moisture in Oklahoma. *Vadose Zone J.* **2017**, *16*, 1–19. [CrossRef]

30. Prasad, R.; Deo, R.C.; Li, Y.; Maraseni, T. Soil moisture forecasting by a hybrid machine learning technique: ELM integrated with ensemble empirical mode decomposition. *Geoderma* **2018**, *330*, 136–161. [CrossRef]

31. Carranza, C.; Nolet, C.; Pezij, M.; van der Ploeg, M. Root zone soil moisture estimation with Random Forest. *J. Hydrol.* **2021**, *593*, 125840. [CrossRef]

32. Kornelsen, K.C.; Coulibaly, P. Root-zone soil moisture estimation using data-driven methods. *Water Resour. Res.* **2014**, *50*, 2946–2962. [CrossRef]

33. Albergel, C.; Rüdiger, C.; Pellarin, T.; Calvet, J.C.; Fritz, N.; Froissard, F.; Suquia, D.; Petitpa, A.; Piguet, B.; Martin, E. From near-surface to root-zone soil moisture using an exponential filter: An assessment of the method based on in-situ observations and model simulations. *Hydrol. Earth Syst. Sci.* **2008**, *12*, 1323–1337. [CrossRef]

34. Wagner, W.; Lemoine, G.; Rott, H. A Method for Estimating Soil Moisture from ERS Scatterometer and Soil Data. *Remote Sens. Environ.* **1999**, *70*, 191–207. [CrossRef]

35. Cho, E.; Choi, M.; Wagner, W. An assessment of remotely sensed surface and root zone soil moisture through active and passive sensors in northeast Asia. *Remote Sens. Environ.* **2015**, *160*, 166–179. [CrossRef]

36. Dumedah, G.; Walker, J.P.; Merlin, O. Root-zone soil moisture estimation from assimilation of downscaled Soil Moisture and Ocean Salinity data. *Adv. Water Resour.* **2015**, *84*, 14–22. [CrossRef]

37. Rouf, T.; Maggioni, V.; Mei, Y.; Houser, P. Towards hyper-resolution land-surface modeling of surface and root zone soil moisture. *J. Hydrol.* **2021**, *594*, 125945. [CrossRef]

38. Wyatt, B.M.; Ochsner, T.E.; Zou, C.B. Estimating root zone soil moisture across diverse land cover types by integrating in-situ and remotely sensed data. *Agric. For. Meteorol.* **2021**, *307*, 108471. [CrossRef]

39. Karandish, F.; Šimůnek, J. A comparison of numerical and machine-learning modeling of soil water content with limited input data. *J. Hydrol.* **2016**, *543*, 892–909. [CrossRef]

40. Ford, T.W.; Harris, E.; Quiring, S.M. Estimating root zone soil moisture using near-surface observations from SMOS. *Hydrol. Earth Syst. Sci.* **2014**, *18*, 139–154. [CrossRef]

41. Wang, T.; Franz, T.E.; You, J.; Shulski, M.D.; Ray, C. Evaluating controls of soil properties and climatic conditions on the use of an exponential filter for converting near surface to root zone soil moisture contents. *J. Hydrol.* **2017**, *548*, 683–696. [CrossRef]

42. Wang, X.; Lü, H.; Crow, W.T.; Zhu, Y.; Wang, Q.; Su, J.; Zheng, J.; Gou, Q. Assessment of SMOS and SMAP soil moisture products against new estimates combining physical model, a statistical model, and in-situ observations: A case study over the Huai River Basin, China. *J. Hydrol.* **2021**, *598*, 126468. [CrossRef]

43. Gou, Q.; Zhu, Y.; Horton, R.; Lü, H.; Wang, Z.; Su, J.; Cui, C.; Zhang, H.; Wang, X.; Zheng, J.; et al. Effect of climate change on the contribution of groundwater to the root zone of winter wheat in the Huaibei Plain of China. *Agric. Water Manag.* **2020**, *240*, 106292. [CrossRef]

44. Su, J.; Lü, H.; Zhu, Y.; Cui, Y.; Wang, X. Evaluating the hydrological utility of latest IMERG products over the Upper Huaihe River Basin, China. *Atmos. Res.* **2019**, *225*, 17–29. [CrossRef]

45. Yin, Y.; Chen, H.; Zhai, P.; Xu, C.-Y.; Ma, H. Characteristics of summer extreme precipitation in the Huai River basin and their relationship with East Asia summer monsoon during 1960–2014. *Int. J. Climatol.* **2019**, *39*, 1555–1570. [CrossRef]

46. CMA Evaluation of Chinese Ground-Based Precipitation Grid Dataset (V 2.0). 2012. Available online: http://image.data.cma.cn/static/subject/doc/SURF_CLI_CHN_PRE_MON_GRID_0.5_ASSESSMENT.pdf (accessed on 1 October 2015). (In Chinese)

47. CMA Evaluation of Chinese Ground-Based Air Temperature Grid Dataset (V 2.0). 2012. Available online: https://www.ckcest.cn/default/es3/detail/4004/dw_dataset/cccc30b0dcc368d608cd0c9db2dd5647 (accessed on 1 October 2015). (In Chinese)

48. Shangguan, W.; Dai, Y.J.; Liu, B.Y.; Zhu, A.X.; Duan, Q.Y.; Wu, L.Z.; Ji, D.Y.; Ye, A.Z.; Yuan, H.; Zhang, Q. A China data set of soil properties for land surface modeling. *J. Adv. Model. Earth Syst.* **2013**, *5*, 212–224. [CrossRef]

49. Reichle, R.H.; Liu, Q.; Koster, R.D.; Crow, W.T.; De Lannoy, G.J.M.; Kimball, J.S.; Ardizzone, J.V.; Bosch, D.; Colliander, A.; Cosh, M.; et al. Version 4 of the SMAP Level-4 Soil Moisture Algorithm and Data Product. *J. Adv. Model. Earth Syst.* **2019**, *11*, 3106–3130. [CrossRef]

50. Albergel, C.; Rüdiger, C.; Carrer, D.; Calvet, J.C.; Fritz, N.; Naeimi, V.; Bartalis, Z.; Hasenauer, S. An evaluation of ASCAT surface soil moisture products with in-situ observations in Southwestern France. *Hydrol. Earth Syst. Sci. Discuss.* **2009**, *13*, 115–124. [CrossRef]

51. Stroud, P.D. *A Recursive Exponential Filter for Time-Sensitive Data*; Los Alamos National Laboratory: Los Alamos, NM, USA, 1999; LAUR-99-5573. Available online: https://www.researchgate.net/publication/242230998_A_Recursive_Exponential_Filter_For_Time-Sensitive_Data (accessed on 3 January 2023).

52. Wang, T.; Franz, T.E.; Zlotnik, V.A. Controls of soil hydraulic characteristics on modeling groundwater recharge under different climatic conditions. *J. Hydrol.* **2014**, *521*, 470–481. [CrossRef]

53. Brocca, L.; Hasenauer, S.; Lacava, T.; Melone, F.; Moramarco, T.; Wagner, W.; Dorigo, W.; Matgen, P.; Martínez-Fernández, J.; Llorens, P.; et al. Soil moisture estimation through ASCAT and AMSR-E sensors: An intercomparison and validation study across Europe. *Remote Sens. Environ.* **2011**, *115*, 3390–3408. [CrossRef]

54. Xing, Z.; Fan, L.; Zhao, L.; De Lannoy, G.; Frappart, F.; Peng, J.; Li, X.; Zeng, J.; Al-Yaari, A.; Yang, K.; et al. A first assessment of satellite and reanalysis estimates of surface and root-zone soil moisture over the permafrost region of Qinghai-Tibet Plateau. *Remote Sens. Environ.* **2021**, *265*, 112666. [CrossRef]

55. Taylor, C.M.; de Jeu, R.A.; Guichard, F.; Harris, P.P.; Dorigo, W.A. Afternoon rain more likely over drier soils. *Nature* **2012**, *489*, 423–426. [CrossRef]

56. Shukla, J.; Mintz, Y. Influence of Land-Surface Evapotranspiration on the Earth's Climate. *Science* **1982**, *215*, 1498–1501. [CrossRef] [PubMed]

57. Findell, K.L.; Eltahir, E. Atmospheric Controls on Soil Moisture–Boundary Layer Interactions. Part II: Feedbacks within the Continental United States. *J. Hydrometeor.* **2003**, *4*, 570–583. [CrossRef]

58. Taylor, C.M.; Parker, D.J.; Harris, P.P. An observational case study of mesoscale atmospheric circulations induced by soil moisture. *Geophys. Res. Lett.* **2007**, *34*, L15801. [CrossRef]

59. Zha, L.; Wu, K.; Li, L.; Cheng, J.; Ju, B. The Cultivation Obstacle Factors of Lime Concretion Black Soil Genuses in Henan. *Chin. J. Soil Sci.* **2013**, *46*, 280–286. [CrossRef]

60. Ceballos, A.; Scipal, K.; Wagner, W.; Martínez-Fernández, J. Validation of ERS scatterometer-derived soil moisture data in the central part of the Duero Basin, Spain. *Hydrol. Process.* **2005**, *19*, 1549–1566. [CrossRef]

61. Reichle, R.H.; De Lannoy, G.J.M.; Liu, Q.; Ardizzone, J.V.; Colliander, A.; Conaty, A.; Crow, W.; Jackson, T.J.; Jones, L.A.; Kimball, J.S.; et al. Assessment of the SMAP Level-4 Surface and Root-Zone Soil Moisture Product Using In Situ Measurements. *J. Hydrometeor.* **2017**, *18*, 2621–2645. [CrossRef]